Competition of two-ion and single-ion anisotropy in rare-earth systems: Large anisotropy example of Tb_5Ge_3

M. Doerr,* A. Haase,† and M. Loewenhaupt
Institut für Festkörperphysik, Technische Universität Dresden, D-01062 Dresden, Germany

M. Rotter
Department of Physics, Clarendon Laboratory, University of Oxford, Parks Road, Oxford OX1 3PU, United Kingdom

M. Bartkowiak
Hochfeld-Magnetlabor Dresden, FZ Dresden-Rossendorf e.V., PF 510119, D-01314 Dresden, Germany

R. Daou†
Max Planck Institute for Chemical Physics of Solids, Nöthnitzer Str. 40, D-01187 Dresden, Germany

E. Kampert and J. A. A. J. Perenboom
Institute for Molecules and Materials, High Field Magnet Laboratory, Radboud University Nijmegen, Toernooiveld 7, NL-6525 ED Nijmegen, The Netherlands

T. Tsutaoka
Department of Science Education, Graduate School of Education, Hiroshima University, 1-1-1 Kagamiyama, Higashi-Hiroshima 739-8524, Japan

(Received 23 April 2010; published 21 July 2010)

The standard model of rare-earth magnetism assumes that magnetic anisotropy is mainly caused by single-ion effects. The importance of two-ion anisotropy is still disputed. For a number of materials this two-ion anisotropy is in the same order of magnitude and strongly influences the magnetic properties. Single crystalline Tb_5Ge_3 has a high moment and low symmetry and, because of this, a large anisotropy is expected. In the present study the influence of the two-ion interaction was investigated. Magnetization and magnetostriction were measured in high magnetic fields up to 60 T. The magnetic phase diagram constructed for the main crystallographic directions shows antiferromagnetism in zero field and a number of magnetic phases at higher fields. The exchange interaction was evaluated based on a model calculation of these phase diagrams. We conclude that a huge anisotropy in the two-ion interaction is present, which overwhelms the single-ion effects.

DOI: 10.1103/PhysRevB.82.024422 PACS number(s): 75.30.Et, 75.30.Kz, 75.80.+q

I. INTRODUCTION

Most members of the R_5Ge_3 (R=rare earth) series are unconventional antiferromagnets (AFs) with complex magnetic structure and a strong interplay of crystallographic and magnetic properties. The R^{3+} moments are located on two different crystallographic sites: one third are on the $4d$ site and two thirds on the $6g$ site of the hexagonal structure (space group $P6_3/mcm$). In the special case of Tb_5Ge_3, the lattice parameters are a=8.495 Å and c=6.351 Å.[1] The compound orders antiferromagnetically at T_N=85 K and the lower susceptibility along the hexagonal axis compared to that in the plane indicates that there is a magnetic easy plane.[2] The magnetic structure at zero field was analyzed by neutron powder diffraction.[3] It suggests a sinusoidally modulated collinear magnetic ordering at T_N with the moments oriented in the a [$(10\bar{1}0)$ in hexagonal notation] direction when they are projected into the basal plane and slightly canted toward the (0001) direction. The propagation vector is τ=(0 0 0.5) which shifts with decreasing temperature, reaching a value of τ=(0 0 0.4616) at about T_t=50 K, which then stays constant down to low temperatures. The low-temperature phase is characterized by a flat spiral with a helical angle of 166.14° between second-nearest neighbors. New neutron-diffraction experiments on a single crystal conclude that the commensurate magnetic structure is stable up to T_N with the propagation vector of about τ=(0 0 0.49).[4] These complex magnetic structures make Tb_5Ge_3 an excellent example for a study of magnetic exchange interactions.

Magnetization studies of Tb_5Ge_3 (and Pr_5Ge_3) have been reported for the $(10\bar{1}0)$ and (0001) directions.[5] The magnetic phase diagram for fields along $(10\bar{1}0)$ shows three more antiferromagnetic phases up to the saturation field of H_a^S=9 T. It is interesting to note that the compound does not undergo a second magnetic transition in zero field at T_t in Ref. 5 as proposed in Ref. 3. However, a wide variety of magnetic modifications below 50 K exist in fields parallel to $(10\bar{1}0)$. All data for fields along the hexagonal (0001) axis clearly show the reorientation of the magnetic moments near T_t.

All these experimental facts require further experimental and theoretical investigation in order to understand the complexity of magnetism in more detail. Measurements of magnetization in all three main crystallographic directions are necessary to construct the magnetic phase diagrams for all these directions. In this way, not only the anisotropy between hexagonal axis and basal plane can be analyzed but also

anisotropy effects in the plane itself. Furthermore, the theoretical evaluation of the exchange interaction, which takes into account isotropic exchange, the dipolar interaction and anisotropic two-ion exchange effects, gives insight into the microscopic properties. In particular, the ratio of the two-ion and single-ion (or crystal-field) anisotropy energies in rare-earth systems is of fundamental interest.

II. SAMPLES AND EXPERIMENTAL

The single-crystalline samples of Tb_5Ge_3 were grown by Czochralski method from single-phase polycrystalline samples using a tri-arc furnace. After a special heat treatment the output crystal was checked and found to be single phase (with impurities less than 1%) by x-ray powder diffraction. Details of the sample preparation are given in Ref. 2. The crystal was cut into smaller pieces with characteristic dimensions of about 2 mm for the magnetization and magnetostriction experiments at moderate fields and of about 0.5 mm for the high-field investigations.

The magnetic properties of Tb_5Ge_3 were studied by magnetization measurements in the temperature range between 2 and 100 K and in magnetic fields up to 14 T using a Quantum Design physical properties measurement system equipped with a vibrating sample magnetometer. The high-field magnetization measurements were carried out up to 60 T in a pulsed magnet with an inductive system with a coil diameter of 1 mm in order to have a high filling factor. The rise time of the pulse magnet was about 10 ms.

Sensitive capacitive dilatometers were used to determine the magnetoelastic properties: the thermal expansion between 1.5 and 300 K and magnetostriction in steady fields (superconducting 15 T magnet at the TU Dresden, resistive Bitter 33 T magnet at the HFML Nijmegen) was measured by a tilted plate capacitive dilatometer[6] with a resolution of relative length changes of 10^{-7}, whereas the parallel-plate dilatometer[7] was the appropriate device for the pulsed field experiments (resolution 10^{-5}).

A. Magnetization

The magnetization of Tb_5Ge_3 at a constant field of 2 T and as a function of temperature is shown in Fig. 1. The magnetization curves in a magnetic field oriented parallel to the three main crystallographic directions at various temperatures between 2 and 100 K are presented in Fig. 2. The maximum of the temperature-dependent magnetization agrees with the antiferromagnetic ordering temperature of 85 K. It is interesting to note that in (0001) direction this peak is split, characterized by two kinks at about 81 and 93 K. This may be a consequence of separate ordering of the Tb^{3+} moments on the 4*d* and 6*g* sites caused by strong anisotropic terms in the two-ion *R*-*R* exchange interaction. The (0001) curve shows another hump at about 50 K which coincides with the change in the magnetic structure discussed below. Small kinks in the $(10\bar{1}0)$ and $(11\bar{2}0)$ curves also are connected to magnetic structure modifications but these modifications only occur when a field of about 2 T is applied and are not present in zero field (not shown here).

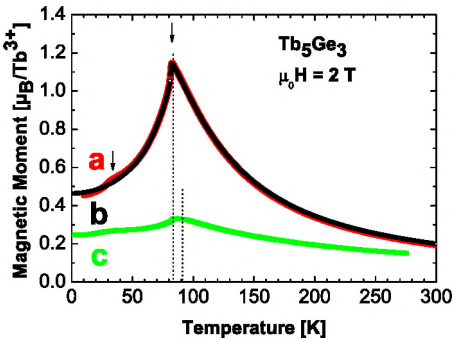

FIG. 1. (Color online) Magnetization of a Tb_5Ge_3 single crystal parallel to the main crystallographic axes *a* [=$(10\bar{1}0)$], *b* [=$(11\bar{2}0)$], and *c* [=(0001)] as a function of temperature in a magnetic field of 2 T.

The isothermal magnetization curves for the $(10\bar{1}0)$ direction confirm the behavior previously analyzed in Ref. 5. The curves for temperatures below 50 K indicate a number of steps associated with the transitions between several (a maximum of three) antiferromagnetic (or ferrimagnetic) phases. The transitions around 3 and 5 T are connected to small magnetization changes. These small anomalies again may be caused by the two different crystallographic sites of the Tb^{3+} ions. Another possibility is to attribute them to reorientations of the low-temperature helical structure. The proposed helical angle between second-nearest neighbors[3] of approximately but not exactly 180° allows a variety of incommensurate magnetic structures in field. Whereas the low-field phases probably result from a change in this angle, the high-field phase is proposed to be of spin-flop character. It is characterized by a difference of the transition fields in the up and down curves. The saturation field in $(10\bar{1}0)$ direction was difficult to estimate (because of the spin-flop state). We estimate that it should be in the range 10–15 T. All these different phases do not exist above 50 K as a result of the rather stable collinear magnetic structure.

Surprisingly, the measurements along $(11\bar{2}0)$ do not resemble the $(10\bar{1}0)$ findings. The three antiferromagnetic low-temperature phases are still present but the highest magnetization increase is at 7 T followed by an additional small jump at 11 T nearly into the saturated state. The hysteresis is more pronounced below 5 K and the saturation field is approximately 14 T. A strong anisotropy should therefore also exist in the hexagonal plane.

The magnetization behavior along (0001) (the hard axis of the system) indicates a phase transition at 5 T in the presence of a nearly linear magnetization slope which is attributed to a smooth rotation of the moments into this direction. The saturation field in the (0001) direction H_c^S is too high to detect directly by magnetization experiments. The magnetization measurements were extended to high fields at 4 K (see Fig. 3). Although the magnetization in high field can be influenced by crystal-field effects, a linear extrapolation of the measured curves to the full moment is a good approximation of this saturation, resulting in a value of about 80 T.

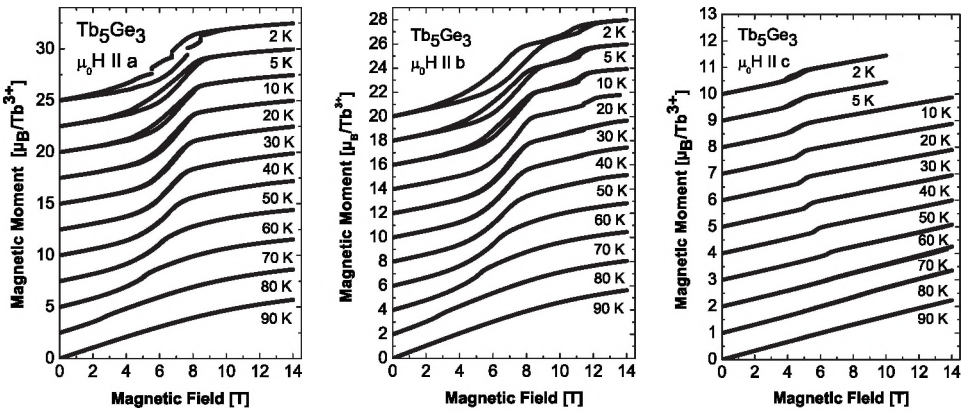

FIG. 2. Magnetization of a Tb_5Ge_3 single crystal as a function of magnetic field parallel to the main crystallographic axes a [=(10$\bar{1}$0), left], b [=(11$\bar{2}$0), center], and c [=(0001), right]. Note: the curves are plotted with offset in order to make clear the temperature dependence.

B. Magnetostriction

The fundamental trend of the thermal expansion and longitudinal magnetostriction curves, shown in Figs. 4 and 5, agrees well with that of the magnetization. The transition temperatures and fields were again determined from anomalies, here kinks or bends in the measured curves, which could be analyzed in detail by taking a derivative of the curves with respect to temperature or magnetic field, respectively. In the thermal-expansion (=zero field) curves only one critical temperature T_N is observed. Summarizing the data along all directions, the spontaneous volume striction below T_N is small with an absolute value of about 10^{-5}. The field-dependent transitions are well pronounced in the longitudinal magnetostriction data: it is possible to identify anomalies at 3.0, 4.9, 7.5, and 8.8 T [(10$\bar{1}$0) axis], 3.1, 8.0, 10.0, and 11.3 T [(11$\bar{2}$0) axis], and 4.2 T [(0001) axis] for increasing field scans at 5 K. A very large effect of about 10^{-3} occurs along the (10$\bar{1}$0) and (11$\bar{2}$0) axes at the highest of these fields which suggests a drastic change in the magnetic structures at these fields whereas the other, smaller, transitions can be modeled as variations in the zero-field structure. The (10$\bar{1}$0) axis transition at about 9 T is very broad which may be understood if the (10$\bar{1}$0) axis oriented moments undergo a spin-flop transition here. Again, the low-temperature transitions are hysteretic. Measurements of the magnetostriction made in high steady and pulsed magnetic fields up to 60 T show no further transitions for fields oriented along any of the principal axes.

III. MAGNETIC PHASE DIAGRAM

The magnetic phase diagrams of Tb_5Ge_3 (see Figs. 6–8) were determined using the measurements of magnetization and magnetostriction. The transition lines created by magnetization resemble those of magnetostriction very well.

The magnetic phase diagrams of the (10$\bar{1}$0) and (11$\bar{2}$0) directions show three ferrimagnetic phases below 50 K in addition to the antiferromagnetic low-temperature phase AF. Taking the proposed spiral structure as the basis, all these phases may be explained by modifications of the angles between neighboring moments. The phase line between AF and the lowest lying ferrimagnetic phase does not seem to be closed and stops at about 50 K. Because the anomalies are small, in magnetization as well as in magnetostriction, this low-field phase transition may be attributed to a separate ordering of the two Tb^{3+} sublattices (as detected by a number of marginal effects before). In contrast, the phase lines between the other ferrimagnetic phases and all others are closed and go directly into the induced ferromagnetic state. The vanishing of the spiral structure modifications above 50 K confirms the tendency to form a more linear magnetic structure at higher temperatures. However, the application of a magnetic field along (10$\bar{1}$0) does not effect the same be-

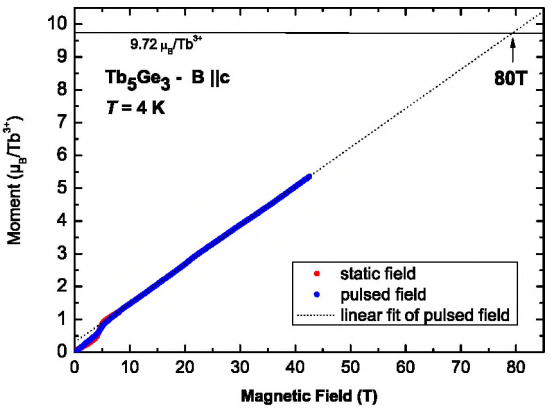

FIG. 3. (Color online) High-field magnetization at 4 K for a magnetic field parallel to the c [=(0001)] axis.

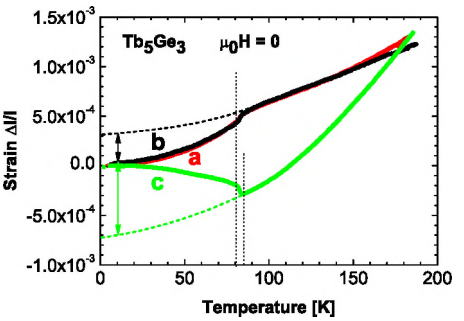

FIG. 4. (Color online) Thermal expansion of a Tb_5Ge_3 single crystal parallel to the main crystallographic axes a [=(10$\bar{1}$0)], b [=(11$\bar{2}$0)], and c [=(0001)] as a function of temperature in zero field.

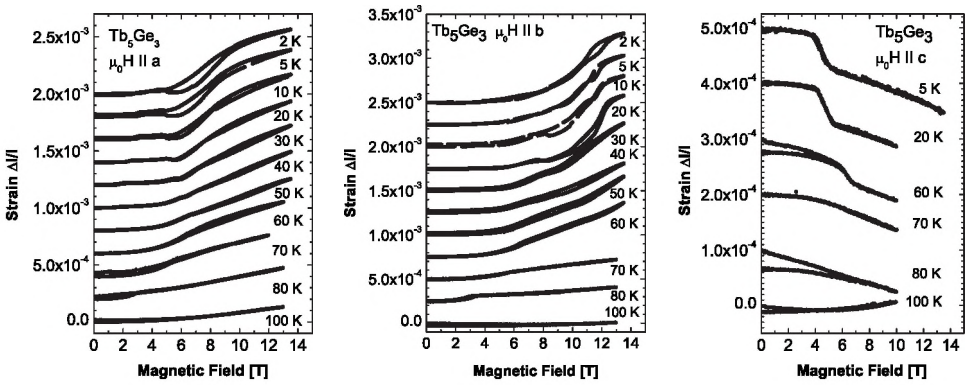

FIG. 5. Forced longitudinal magnetostriction of a Tb_5Ge_3 single crystal parallel to the main crystallographic axes a [=(10$\bar{1}$0), left], b [=(11$\bar{2}$0), center], and c [=(0001), right]. Note: the curves are plotted with offset in order to make clear the temperature dependence.

havior as a magnetic field along (11$\bar{2}$0). As discussed above, a field of approximately 8 T along (10$\bar{1}$0) induces a spin-flop phase. Therefore, saturation in the (10$\bar{1}$0) direction requires a higher field (continuous transition into the induced ferromagnetism). This observed anisotropy in the basal plane of the hexagonal structure can be understood theoretically in a model including anisotropic two-ion interactions (see below). The phase diagram along the (0001) direction is characterized by a steady rotation of the magnetic moments. There is a transition line around 5 T, deduced from magnetization and magnetostriction jumps, but saturation needs very high fields because of the strong anisotropy of Tb^{3+}.

IV. THEORETICAL MODEL

A. Basic considerations of anisotropy

A first theoretical step to calculate the saturation fields can be performed using the high-temperature approximation of the susceptibility measurements,[2] which gives the paramagnetic Curie temperatures to be Θ_a=60 K and Θ_c=−100 K, approximately. Following the formalism[8] (which is strictly valid only for a one-atom unit cell and assumes that the difference of the paramagnetic Curie temperatures is determined by only the crystal-field parameter B_2^0) the paramagnetic Curie and the magnetic ordering temperatures can be written as

$$\Theta_a = \frac{J(J+1)}{3k_B}\mathcal{J}_{aa}(q=0) + \frac{2}{5k_B}\left(J-\frac{1}{2}\right)\left(J+\frac{3}{2}\right)B_2^0, \quad (1)$$

$$\Theta_c = \frac{J(J+1)}{3k_B}\mathcal{J}_{cc}(q=0) - \frac{4}{5k_B}\left(J-\frac{1}{2}\right)\left(J+\frac{3}{2}\right)B_2^0, \quad (2)$$

$$T_N = \frac{J(J+1)}{3k_B}\mathcal{J}_{aa}(q=\tau)\left[1+\frac{2}{5k_B}\left(J-\frac{1}{2}\right)\left(J+\frac{3}{2}\right)\frac{B_2^0}{k_B T_N}\right]. \quad (3)$$

Using at first an isotropic two-ion interaction for reasons of simplicity (i.e., $\mathcal{J}_{aa}=\mathcal{J}_{cc}=:\mathcal{J}$) and inserting the experimental values Θ_a=60 K and Θ_c=−100 K and J=6 for Tb^{3+} in Eqs. (1) and (2) this leads to a value B_2^0=0.28 meV. Inserting the experimental value of the Néel temperature T_N into Eq. (3) allows us to evaluate the Fourier transform of the two-ion interaction at the wave vector $\mathcal{J}(q=\tau)$. Together with $\mathcal{J}(q=0)$ calculated from Eqs. (1) and (2) the saturation field can be computed,[9]

$$H^S = \frac{J}{g_J\mu_B}[\mathcal{J}(q=\tau) - \mathcal{J}(q=0)]. \quad (4)$$

Thus the saturation field in (10$\bar{1}$0) direction is given by

$$H_a^S = 3k_B\frac{T_N - \Theta_a}{g_J\mu_B(J+1)}. \quad (5)$$

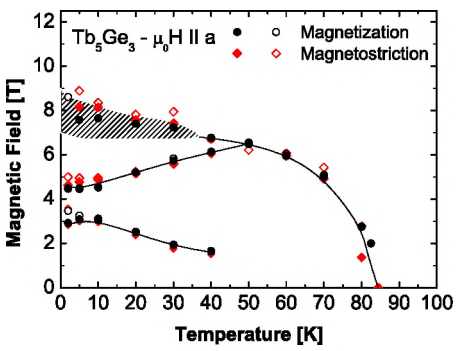

FIG. 6. (Color online) Magnetic phase diagram of Tb_5Ge_3 for an external field oriented along (10$\bar{1}$0) as constructed from magnetization (circles) and magnetostriction (diamonds). The open and closed symbols represent the transitions found at increasing or decreasing field sweeps, respectively.

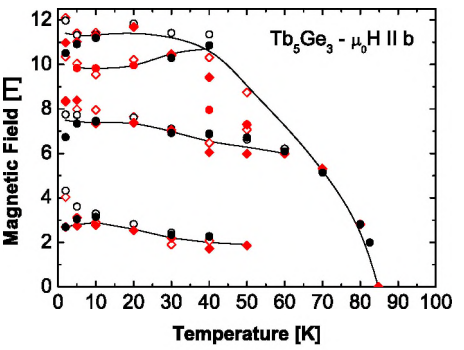

FIG. 7. (Color online) Magnetic phase diagram of Tb_5Ge_3 for an external field oriented along (11$\bar{2}$0) as constructed from magnetization (circles) and magnetostriction (diamonds).

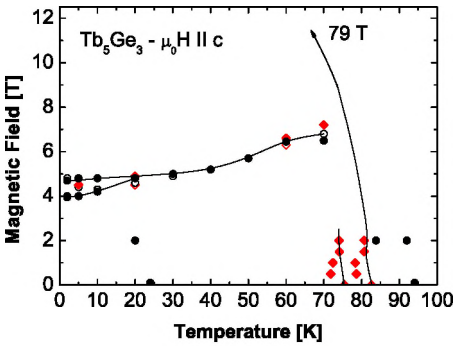

FIG. 8. (Color online) Magnetic phase diagram of Tb_5Ge_3 for an external field oriented along (0001) as constructed from magnetization (circles) and magnetostriction (diamonds).

Inserting experimental values for T_N and Θ_a gives $H_a^S = 23$ T. This value is much too high in comparison to the experimental data and illustrates the discrepancy between the experimental results and the (still simple) model, in other words: in the framework of Eqs. (1)–(5) no congruence of the saturation field and transition temperatures could be reached.

Because of this, the calculation was repeated assuming an anisotropic two-ion interaction $\mathcal{J}_{aa}$ and J_{cc} and neglecting (to avoid confusion between the different anisotropy parts) the single-ion anisotropy (i.e., $B_2^0 = 0$). Using again Eqs. (1)–(3) with $B_2^0 = 0$ the saturation fields can be estimated from Eq. (5) and the equivalent expression

$$H_c^S = 3k_B \frac{T_N - \Theta_c}{g_J \mu_B (J+1)}, \tag{6}$$

which gives $H_a^S = 10$ T and $H_c^S = 79$ T. These values are in very good agreement with the experimental data. This good match suggests a very small crystal-field influence on the anisotropy in Tb_5Ge_3. Note that in this estimation of the saturation field values we also obtain values for the two-ion interaction: we get $\mathcal{J}_{aa}(q=0) = 0.37$ meV, $\mathcal{J}_{cc}(q=0) = -0.62$ meV, and $\mathcal{J}_{aa}(q=\tau) = 0.52$ meV.

However, these very basic estimations are not sufficient to explain the magnetism of Tb_5Ge_3 in detail. In order to describe the anisotropy (especially within the *ab* plane) and the magnetic structure we have to consider nonzero anisotropy values B_l^m and the complicated crystal structure with different Tb^{3+} positions. A numerical mean-field calculation incorporating this complexity was realized.

B. Model calculation of the magnetic structure

In order to model the magnetic phase diagram of Tb_5Ge_3 for several crystallographic directions the standard model of rare-earth magnetism has been evaluated.[8] The numerical calculations have been performed using the program package MCPHASE.[10] To account for the observed anisotropy effects, the Hamiltonian was expressed as

$$\mathcal{H} = \sum_{i,lm} B_l^m(i) O_l^m(\mathbf{J}_i) - \frac{1}{2}\sum_{ij} \mathbf{J}_i \begin{pmatrix} \mathcal{J}_{aa}(ij) & 0 & 0 \\ 0 & \mathcal{J}_{bb}(ij) & 0 \\ 0 & 0 & \mathcal{J}_{cc}(ij) \end{pmatrix} \mathbf{J}_j - \sum_i g_J \mu_B \mathbf{J}_i \mathbf{H}. \tag{7}$$

In Eq. (7) the different parts denote the single-ion or crystal-field (CEF) effect, the anisotropic two-ion interaction and the Zeeman term. The $B_l^m(i)$ denote the crystal-field parameters of the ion i, the $O_l^m(\mathbf{J}_i)$ are Stevens operator equivalents, g_J is the Landé coupling factor, and $\mathbf{H}$ the applied magnetic field.

First, the single-ion anisotropy was considered. Since no inelastic neutron-scattering data are available, the main crystal-field parameters B_l^m were estimated from a point-charge model. It is necessary to consider the Tb site symmetry properly because of the different B_2^0 and B_2^2 parameters for the 6*g* and 4*d* positions.

Assuming an isotropic magnetic exchange interaction to begin with, the exchange parameters $\mathcal{J}_\gamma$ ($\gamma = aa, bb, cc$) are determined by a parametrized Bethe-Slater curve. However, as expected from the initial considerations above, such a model failed to reproduce the saturation field in plane. Therefore, magnetoelastic interactions were considered but also this model could not explain the magnitude of the magnetic saturation fields.

Therefore in a next step a full theoretical calculation according to Eq. (7) was realized assuming a strong anisotropy of the two-ion interaction. As already seen by the analysis following Eqs. (1)–(4), a solution consistent with the experimental magnetization data only exists for very small single-ion anisotropy. Hence in our model we took point charges of $-0.1|e|$ on neighboring atoms and obtained a very small $B_2^0 = 0.0344$ meV. In this case, according to Eq. (5), the transition field $H_a^S = 14.5$ T is much lower and also the correct temperatures $T_N = 85$ K and $\Theta_a \simeq 60$ K and $\Theta_c \simeq -100$ K are confirmed. In consequence, this means a negligible CEF anisotropy between the hexagonal *ab* plane and the *c* axis compared to that of the magnetic two-ion exchange.

Note that a nonzero CEF anisotropy is necessary within the *ab* plane to describe the anisotropy in the transition fields. There is, for example, still a small B_2^2 on the Tb 6*g* sites in order to get a different magnetization along $(10\bar{1}0)$ and $(11\bar{2}0)$. This results in a saturation field $H_b^S = 11.5$ T. The lower saturation field for the $(11\bar{2}0)$ and the larger one for $(10\bar{1}0)$ is self-explanatory assuming a spin-flop transition in $(10\bar{1}0)$ at about 8 T and the saturation at a field of only $H_a \geq 15$ T.

Finally, the simulation is based on a parametrized Bethe-Slater curve for the two-ion interaction,

$$\mathcal{J}_\gamma(R) = A_\gamma \left(-\frac{R^2}{D_\gamma^2} + \frac{R^4}{D_\gamma^4} \right) \exp(-\alpha_\gamma R^2 / D_\gamma^2) \tag{8}$$

with $\gamma = aa, bb, cc$. We used $A_{aa} = A_{bb} = 1.303$ meV, $D_{aa} = D_{bb} = 6.248/\text{Å}$, $\alpha_{aa} = \alpha_{bb} = 2.404$, $A_{cc} = -0.0383$ meV, $D_{cc} = 5.254/\text{Å}$, and $\alpha_{cc} = 1.248$.

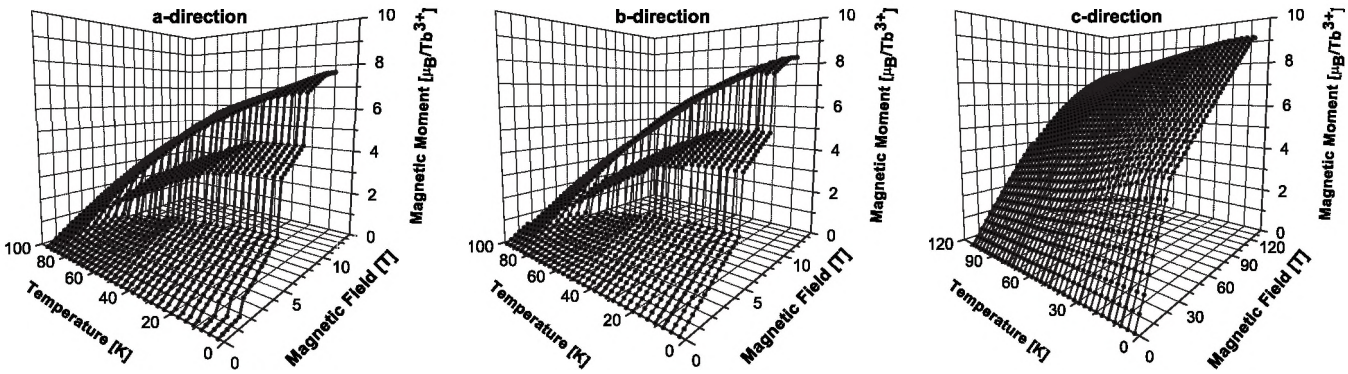

FIG. 9. Isothermal magnetization of a Tb_5Ge_3 single crystal parallel to the main crystallographic axes a [=(10$\bar{1}$0), left], b [=(11$\bar{2}$0), center], and c [=(0001), right] at different temperatures from 2 to 98 K as calculated by the MCPHASE package (the temperature steps between the presented curves are 3 K).

With this parametrization of Hamiltonian (7) the MCPHASE simulation produces the magnetization curves presented in Fig. 9. The calculation of isothermal magnetization resembles the main features of the experimental curves well. The magnetization jumps along (10$\bar{1}$0) are consistent with the anomalies and transitions shown in the phase diagrams. It should be noted that these transitions can have a wide tolerance (especially seen in the phase diagram from the hysteresis at low temperatures) which is connected to the helical magnetic structure with an angle of nearly but not exactly 180°. This special configuration may result in a spin-slip behavior when applying an external magnetic field with no sharp transition fields. Also the calculated temperature dependence of magnetization corresponds well to the experimental data. The Néel temperature has the correct value T_N =83 K and additionally the transition at about 60 K and 2 T which is visible in the phase diagram is pronounced in the calculation.

On the strength of this model calculation it is possible to propose an explanation of the low-temperature magnetic structure of Tb_5Ge_3. Figure 10 shows the orientation of the magnetic Tb^{3+} moments [projected into the (hexagonal) ab plane] at 5 K and its development with external magnetic field parallel to (10$\bar{1}$0) (the structures at 0, 7, and 11 T are shown here). The preferred orientation of the moments parallel to the (10$\bar{1}$0) and (11$\bar{2}$0) axes, respectively, is in accord with the results of the new neutron-diffraction experiments[4] which showed a nearly antiparallel orientation of the moments (helical structure with a characteristic angle close to 180°) and a temperature-independent propagation vector τ =(0 0 0.49). However, the calculated structure is more complex and contains parts, deviating from an easy collinear behavior which more or less reflects the hexagonal symmetry: The moments of the ions at the crystallographic 4d positions are collinear, whereas those of the ions at the 6g positions form a hexagonal structure. Both configurations are characterized by a propagation vector τ=(0 0 0.5). Figure 10 also illustrates the development of the magnetic array with field. The spin-flop transition starts at about 7 T and is not completely finished at 11 T (see right picture). This confirms the idea that magnetic saturation along the (10$\bar{1}$0) axis is not reached below a field of about 15 T (see phase diagram above). Additionally, it becomes clear from the calculation of the magnetic structure that the (10$\bar{1}$0) and (11$\bar{2}$0) directions are not equivalent due to a small CEF anisotropy. Nevertheless, the main points of the magnetic properties are caused by different Tb^{3+} positions combined with an anisotropic magnetic exchange. This may lead to the requirement of experimental reconsideration of the magnetic structure.

The application of a magnetic field turns the moments toward this field direction. The beginning of the spin-flop process along (10$\bar{1}$0) is visible in the 7 T graph. The 11 T graph illustrates that a complete saturation is not yet reached at this field value as found by the basic measurements of magnetization and magnetostriction.

It is worth emphasizing again that the mean-field simulation following Eq. (7) that assumed an isotropic two-ion in-

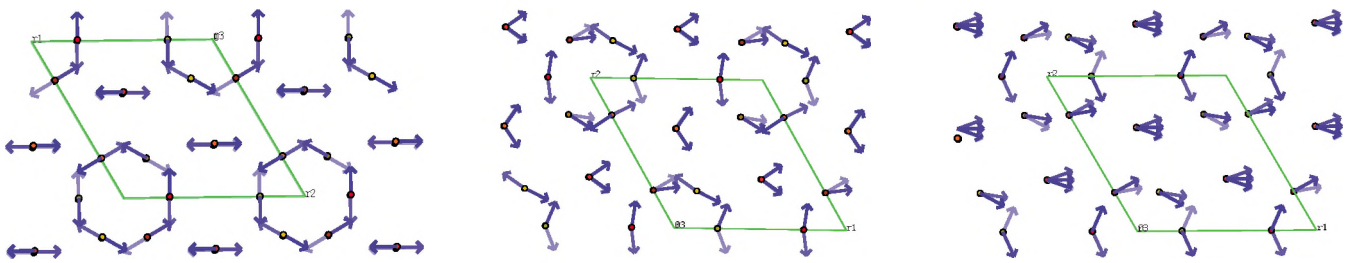

FIG. 10. (Color online) Magnetic structure of Tb_5Ge_3 at T=5 K and magnetic fields of $\mu_0 H$=0 T (left), 7 T (center), and 11 T (right) along the a [=(10$\bar{1}$0) axis] as received from the mean-field calculation. The graphic shows a projection into the hexagonal plane. The differently marked circles denote the Tb^{3+} 4d or 6g sites.

teraction and a single-ion anisotropy could in no case come to a satisfying agreement with the experimental data. In particular, the transition fields that were calculated were much too high. An adequate result can only be achieved assuming a strong anisotropy of the two-ion interaction which is considerably higher than the single-ion effect.

V. CONCLUSIONS

The investigation of the magnetic properties of the hexagonal rare-earth compound Tb_5Ge_3, experimentally based on measurements of magnetization and magnetostriction at a single crystal, results in a complex phase diagram. The moments are oriented in the *ab* plane, so there is an easy plane of magnetization. The compound has an anisotropy not only between hexagonal plane and axis but also in the *ab* plane itself. The experimental and theoretical investigation confirms a temperature-dependent propagation vector of the magnetic structure of approximately $\tau=(0\ 0\ 0.5)$, as found by elastic neutron scattering in a single crystal. Because of this, the magnetic structure is likely to be of spiral type with a characteristic angle close to 180°.

Usually the anisotropy of rare-earth systems is believed to be due to single-ion effects. However, it is known from Gd^{3+} compounds, which have no single-ion anisotropy, that other types of anisotropy (for example, an anisotropic bilinear interaction as of Dzyaloshinskii-Moriya type) are necessary for a reasonable explanation of the magnetic phenomena. The magnetic properties exhibited by Tb_5Ge_3 can only be understood introducing a two-ion anisotropy into the mean-field simulation. This anisotropy was found to be stronger than the single-ion one characterized by a nearly vanishing (averaged) CEF parameter B_2^0. Because of this fact Tb_5Ge_3 is a system in which the single-ion anisotropy seems to be negligible in comparison to a huge anisotropy in the two-ion interaction. This demonstrates the importance of the two-ion anisotropy effects in the analysis of magnetic properties of rare-earth compounds.

Further modeling including the influence of magnetoelastic and biquadratic interactions could possibly improve the description of the experimental data. It will be interesting to see if the model assumptions made here can be confirmed by other experimental studies, such as inelastic or diffuse neutron scattering, electron-spin resonance, or x-ray absorption.

ACKNOWLEDGMENTS

We want to thank the Hiroshima University for providing us with Tb_5Ge_3 single crystals. We acknowledge support by EuroMagNET under Contracts No. 506239 (FP6) and No. 228043 (FP7).

*doerr@physik.tu-dresden.de
†Also at Hochfeld-Magnetlabor Dresden, FZ Dresden-Rossendorf e.V., PF 510119, D-01314 Dresden, Germany.

[1] K. Buschow and J. Fast, Phys. Status Solidi **21**, 593 (1967).
[2] T. Tsutaoka, Y. Nishiume, and T. Tokunaga, J. Magn. Magn. Mater. **272-276**, E421 (2004).
[3] P. Schobinger-Papamantellos, J. Magn. Magn. Mater. **28**, 97 (1982).
[4] T. Tsutaoka, Y. Nishiume, S. Kawano, Y. Andoh, M. Kurisu, and G. Nakamoto, KURRI Prog. Rep. **2003**, 9 (2004).
[5] D. A. Joshi, A. Thamizhavel, and S. K. Dhar, Phys. Rev. B **79**, 014425 (2009).
[6] M. Rotter, H. Müller, E. Gratz, M. Doerr, and M. Loewenhaupt, Rev. Sci. Instrum. **69**, 2742 (1998).
[7] M. Doerr, W. Lorenz, T. Neupert, M. Loewenhaupt, N. V. Kozlova, J. Freudenbeger, M. Bartkowiak, E. Kampert, and M. Rotter, Rev. Sci. Instrum. **79**, 063902 (2008).
[8] J. Jensen and A. R. Mackintosh, *Rare Earth Magnetism* (Clarendon Press, Oxford, 1991).
[9] J. Jensen and M. Rotter, Phys. Rev. B **77**, 134408 (2008).
[10] M. Rotter, J. Magn. Magn. Mater. **272-276**, E481 (2004).